Physica A 389 (2010) 1931–1944

Contents lists available at ScienceDirect

Physica A

journal homepage: www.elsevier.com/locate/physa

Nonequilibrium potential for arbitrary-connected networks of FitzHugh–Nagumo elements

Alejandro D. Sánchez [1], Gonzalo G. Izús [*,1]

IFIMAR, Instituto de Investigaciones Físicas de Mar del Plata (CONICET–UNMdP), Facultad de Ciencias Exactas y Naturales, Universidad Nacional de Mar del Plata, Deán Funes 3350, (7600) Mar del Plata, Argentina

ARTICLE INFO

Article history:
Received 10 October 2009
Received in revised form 19 December 2009
Available online 15 January 2010

Keywords:
Nonequilibrium potential
Antiphase coupling
FitzHugh–Nagumo model

ABSTRACT

We study an array of N units with FitzHugh–Nagumo dynamics linearly coupled. The system is submitted to a subthreshold harmonic signal and independent Gaussian white noises with a common intensity η. In the limit of adiabatic driving, we analytically calculate the system's nonequilibrium potential for arbitrary linear coupling. We illustrate its applicability by investigating noise-induced effects in an excitable regular network with extended antiphase coupling. In particular, the levels of noise for short-wavelength phase-instability, network's synchronization and depinning of "defects" (groups of contiguous inhibited neurons on an antiphase background) are theoretically predicted and numerically confirmed. The origin of these collective effects and the dependence with parameters of the most probable length of defects are explained in terms of the system's nonequilibrium potential.

1. Introduction

The constructive effect of noise in the dynamics of complex systems is a subject of high interest and activity. Examples of such a behavior are seen in phenomena like coherence resonance [1], stochastic resonance [2] or noise-induced synchronization in nonlinear dynamical systems [3]. Of particular relevance is the study of synchronization processes in populations of interacting nonlinear oscillators in order to understand some key issues in neuroscience, where a number of modeling approaches have been based on the description of each single neuron as a relaxation oscillator [4–6].

A single neuron displays excitable behavior, in the sense that small perturbations to its quiescent state (stable stationary state of the cross membrane potential) can lead to a large excursion of its potential. Excitable units usually appear as constitutive elements of complex systems with nontrivial couplings and striking dynamics. For example, there are many studies for excitable networks under external periodic stimuli, both experimentally and theoretically, which show several behaviors including phase locking, synchronization and chaotic dynamics [7–11]. In particular, the problem of synchronization in excitable systems with phase-repulsive or delayed coupling has been extensively considered [7,12–15]. In these systems, the oscillators tend to have a phase opposite to that of their nearest neighbors. Most of the previous studies analyzing the influence of noise on excitable networks are based on numerical investigations [16–19], while the development of theoretical tools are limited by the intrinsic difficulty to solve the related non-potential Fokker–Planck equations, even at the level of an isolated cell [20].

In a previous study [21] we have characterized a noise-induced synchronization of a ring of autonomous units with excitable FitzHugh–Nagumo (FHN) dynamics, coupled to first neighbors in a phase-repulsive way. Particularly, we have

* Corresponding author.
E-mail addresses: sanchez@mdp.edu.ar (A.D. Sánchez), izus@mdp.edu.ar (G.G. Izús).
[1] Member of CONICET, Argentina.

0378-4371/$ – see front matter © 2010 Elsevier B.V. All rights reserved.
doi:10.1016/j.physa.2010.01.013

predicted and numerically confirmed the levels of noise for the system's activation and synchronization. The analysis was done in terms of the nonequilibrium potential (NEP). The NEP is the out of equilibrium analog of a free energy which brings up a deep insight into the dynamical mechanisms leading to pattern formation and other phenomena where fluctuations play a constructive role [22]. In particular, it is the appropriate Lyapunov functional of the deterministic dynamics that provides information on the local and global properties of attractors. For example, it characterizes their linear and nonlinear stability and also determines the height of barriers separating attraction basins, which in turn define the transition rates among attractors [22]. For nonlinear multicomponent systems, however, integrability conditions are a severe obstacle to the analytical finding of the NEP. A recent review [23] summarizes the way where its knowledge for some reaction–diffusion systems has allowed e.g. to explain system-size stochastic resonance without resorting to a mean-field approximation [24], to predict the enhancement of the signal-to-noise ratio by an appropriate nonlinear diffusion coefficient [25], to go beyond the reaction–diffusion approximation in a controlled way [26], etc.

The main purpose of this work is to extend the analysis of Ref. [21] to arbitrary-connected networks of FHN cells by calculating the appropriates NEPs. The objective is to obtain an analytical expression of the NEP that can be used for a wide range of linear couplings. The development of this theoretical tool results appropriated to discriminate between the effects induced by the network topology from the effects induced by noise. To illustrate its applicability, we analyze the stochastic dynamics of regular FHN's networks with extended antiphase coupling. The observed dynamics is interpreted in terms of the corresponding NEPs and the levels of noise for short-wavelength phase-instability, network's synchronization, and length and depinning of "defects" (groups of contiguous inhibited neurons on an antiphase background) are theoretically determined and numerically confirmed.

The paper is organized as follows: Section 2 briefly reviews the dynamical equations of the model. Section 3 presents the theoretical derivation of the NEP. In Section 4 we give numerical evidence of noise-sustained activation and synchronization for systems with extended antiphase coupling. We also present here the characterization of the dynamics in terms of the corresponding NEP, while the conclusions are summarized in Section 5.

2. The model

The FitzHugh Nagumo model is one of the simplified modifications of the widely known Hodgkin–Huxley model. It describes the dynamics of excitable systems in different fields, such as kinetics of chemical reaction and solid state physics [1,16,27–29]. From a theoretical point of view, the FHN model is relatively easy to investigate, nevertheless many effects observed in neural cells are qualitatively contained in it. For example, it has been extremely useful in understanding the dynamics of some neural [30] and cardiac tissues [8], to cite a few examples of biomedical relevance.

In this work we study a network of N identical excitable FHN elements with an arbitrary linear coupling in the activator's components. The cells are submitted to a common subthreshold signal and independent additive Gaussian white noises. The set of dynamical equations for the model is

$$\begin{aligned}\dot{u}_i &= b\,u_i(1-u_i^2) - v_i + S(t) + \sum_{j=1}^{N} D_{ij}\,u_j + r_1\,\xi_i^{(u)}(t) + r_2\,\xi_i^{(v)}(t)\\ \dot{v}_i &= \epsilon(\beta\,u_i - v_i + C) + r_3\,\xi_i^{(u)}(t) + r_4\,\xi_i^{(v)}(t)\end{aligned} \tag{1}$$

where $u_i(t)$ is the fast variable which mimics the action potential of cell (node) i and $v_i(t)$ is the slow – or recovery – variable which is related to the time dependent conductance of the potassium channels in the membrane [31]. Here $S = S_0\sin(\Omega t)$ is the external signal, ϵ is the activator–inhibitor time scales ratio and D_{ij} are the coupling matrix elements which defines the network structure, i.e., the connections among the elements. Throughout the work the following values have been adopted: $N = 256$, $\epsilon = \beta = 0.01$, $b = 0.035$, $C = 0.02$, $S_0 = 0.011$, $\Omega = 0.002$, $\epsilon\,r_1 = r_3 = \cos(0.05)$, $\epsilon\,r_2 = r_4 = \sin(0.05)$ and $D_{ii} = 0$. The values of the parameters are not totally arbitrary. On one hand, Ω remains below the typical inverse deterministic time (i.e. the turnaround time of a single spike), so that the signal can be regarded as an adiabatic perturbation. On the other hand, some parameters were selected in such a way that they satisfy an integrability condition required by the theoretical characterization of the dynamics (see next section). Finally, for the statistical properties of the Gaussian noises $\xi_i^{(u,v)}$ we assume $\langle\xi_i^{(p)}(t)\rangle = 0$ and $\langle\xi_i^{(p)}(t)\,\xi_j^{(q)}(t')\rangle = 2\eta\ \delta_{i,j}\,\delta_{p,q}\,\delta(t-t')$, where η is the common noise intensity and $p, q \in \{u, v\}$. Note that the structure of the noise terms is the more general structure that the Langevin theory allows for a single two-component neuron (system) subjected to additive noise [32]. Neurons are then linked to form a network without introduce additional randomness.

In the absence of driving, coupling and noise there is only one – uniform – steady state, determined by the rest state of the isolated excitable cell. The external signal only induces small subthreshold oscillations around this state. Linear coupling open the possibility to observe dephasing and antiphase phase locking in coupled excitable systems [33]. In particular, for $D_{ij} = -D\,(\delta_{i,j+1} + \delta_{i,j-1})$ with $D > 0$, we have showed that networks can exhibit a noise-sustained synchronization of an antiphase state with the external signal [21]. The observed dynamics was elucidated in terms of noise-induced transitions among attractors, being a fundamental ingredient the changes in the relative stability, which are determined by the NEP. To generalize those results to more general couplings, we first review the concept of nonequilibrium potential and we sketch its derivation for Eq. (1).

3. The nonequilibrium potential

For Langevin-type dynamics, Graham and collaborators have defined the NEP $\mathcal{F}$ in terms of the zero-noise limit of the logarithm of the stationary probability density function (see references in Ref. [22]). For Eq. (1), the steady state distribution takes the form

$$P_s(\{u_i, v_i\}, \eta) = Z(\{u_i, v_i\}) \exp\left[-\frac{\mathcal{F}(\{u_i, v_i\})}{\eta} + \mathcal{O}(\eta)\right]. \tag{2}$$

Following Graham [22], equations for $\mathcal{F}(\{u_i, v_i\})$ and $Z(\{u_i, v_i\})$ are obtained from the stationary Fokker–Plank equation corresponding to Eq. (1). In particular, the NEP satisfies the nonlinear first order partial differential equation

$$\sum_{i=1}^{N}\left[\varphi_{u_i}\partial_{u_i}\mathcal{F} + \varphi_{v_i}\partial_{v_i}\mathcal{F} + \frac{1}{2}\lambda_1(\partial_{u_i}\mathcal{F})^2 + \lambda\partial_{u_i}\mathcal{F}\,\partial_{v_i}\mathcal{F} + \frac{1}{2}\lambda_2(\partial_{v_i}\mathcal{F})^2\right] = 0, \tag{3}$$

where

$$\varphi_{u_i} = b\,u_i(1-u_i^2) - v_i + S(t) - \sum_{j=1}^{N} D_{ij}\,u_j \quad \text{and}$$
$$\varphi_{v_i} = \epsilon\,(\beta\,u_i - v_i + C) \tag{4}$$

are the components of the deterministic phase-space flow in Eq. (1), and

$$\lambda_1 = r_1^2 + r_2^2, \tag{5}$$
$$\lambda_2 = r_3^2 + r_4^2 \quad \text{and} \tag{6}$$
$$\lambda = r_1 r_3 + r_2 r_4 \tag{7}$$

are the system's transport matrix elements of the associated Fokker–Planck Equation. In addition, the prefactor Z satisfies the linear partial differential equation depending on $\mathcal{F}(\{u_i, v_i\})$

$$\sum_{i=1}^{N}\Bigg[(\varphi_{u_i} + \lambda_1\partial_{u_i}\mathcal{F} + \lambda\partial_{v_i}\mathcal{F})\,\partial_{u_i}Z + (\varphi_{v_i} + \lambda\partial_{u_i}\mathcal{F} + \lambda_2\partial_{v_i}\mathcal{F})\,\partial_{v_i}Z + \left(\partial_{u_i}\varphi_{u_i} + \partial_{v_i}\varphi_{v_i} + \frac{\lambda_1}{2}\partial^2_{u_i^2}\mathcal{F} + \lambda\partial^2_{u_iv_i}\mathcal{F} + \frac{\lambda_2}{2}\partial^2_{v_i^2}\mathcal{F}\right)Z\Bigg] = 0. \tag{8}$$

Analytical expressions of $\mathcal{F}$ and Z have been obtained for some version of the isolated [20,34] and nearest-neighbor spatially coupled FHN systems [21,35,36]. In order to solve Eq. (3), the deterministic phase-space flow is decomposed into a sum of a dissipative $\varphi^d_{u_i,v_i}$ and a conservative $\varphi^c_{u_i,v_i}$ components, in such a way that $\{\varphi^c_{u_i}, \varphi^c_{v_i}\}$ conserves the potential $\mathcal{F}$, i.e.

$$\sum_{i=1}^{N}(\varphi^c_{u_i}\partial_{u_i}\mathcal{F} + \varphi^c_{v_i}\partial_{v_i}\mathcal{F}) = 0. \tag{9}$$

As in Ref. [20], we propose

$$\varphi^d_{u_i} = -\frac{1}{2}(\lambda_1\partial_{u_i}\mathcal{F} + \lambda\partial_{v_i}\mathcal{F})$$
$$\varphi^d_{v_i} = -\frac{1}{2}(\lambda\partial_{u_i}\mathcal{F} + \lambda_2\partial_{v_i}\mathcal{F}) \tag{10}$$

and

$$\varphi^c_{u_i} = -\frac{1}{2}\lambda\partial_{v_i}\mathcal{F}$$
$$\varphi^c_{v_i} = \frac{1}{2}\lambda\partial_{u_i}\mathcal{F}. \tag{11}$$

With this election equation (9) is satisfied and the Lyapunov-functional property of $\mathcal{F}$ for the deterministic dynamics is verified. Following the calculations of Ref. [21], we find

$$\mathcal{F}(\{u_j, v_j\}) = \sum_{i=1}^{N}\mathcal{F}_s(u_i, v_i) + \frac{1}{\lambda_1}\sum_{i=1}^{N}\sum_{j=1}^{N}D_{ij}u_iu_j, \tag{12}$$

where

$$\mathcal{F}_s(u_i, v_i) = \frac{\epsilon}{\lambda_2}(v_i^2 - 2\beta\, u_i v_i - 2C v_i) + \frac{2\lambda\epsilon}{\lambda_1\lambda_2}(\beta\, u_i^2 + 2C u_i) - \frac{2}{\lambda_1}\left[\frac{b}{2}u_i^2 - \frac{b}{4}u_i^4 + S(t)\, u_i\right] \tag{13}$$

is the NEP of a single cell [20]. From Eq. (8) the prefactor Z results to be a constant which can be fixed by normalization. Integrability conditions constrain the parameters to obey

$$\beta\lambda_1 + \lambda_2/\epsilon = 2\lambda \quad \text{and} \tag{14}$$

$$D_{ij} = D_{ji}. \tag{15}$$

For Eq. (1) relation (14) can be fulfilled for selected values of parameters, both in the excitable and the bistable regimes. Note that $\{r_i\}$ does not determine the value of η but only the structure of the transport matrix in the $2N$-dimensional Fokker–Planck equation. In the same sense, the coupling matrix $\{D_{ij}\}$ is an arbitrary but symmetric matrix which originates a non-local structure for both, the dissipative and the conservative components of the phase-space flow. In Eq. (12) we can see that $\mathcal{F}$ has two contributions, the first one is given by the NEP of isolated cells, while the second one (the non-local contribution) originates a u-quadratic form that take into account the topology of the network.

Finally, we remark the explicit dependence of $\mathcal{F}$ on t, caught up by each u_i variable through its coupling to the external signal. This is consistent with the NEP calculation only in the adiabatic limit, i.e. for Ω so small that the probability distribution permanently accommodates into its stationary condition. In other words, the t-dependence of $\mathcal{F}$ is parametric.

4. Networks with extended antiphase coupling

By extended antiphase coupling (EAC) we mean groups of neurons coupled among them in such a way that the antiphase configuration is globally favored. An EAC can be obtained in a ring through the linear coupling $D_{ij} = -D$ for $1 \le i \le N$ with j increasing in step two into the range $i - (2k-1) \le j \le i + (2k-1)$, and $D_{ij} = 0$ otherwise. Here k denotes the number of one-sided coupled cells to the cell i, and $2k-1$ is the coupling's range. Note that D_{ij} couples only odd neighbors, in order to enforce the antiphase configuration. The case $k = 1$ was considered in Ref. [21]. The proposed EAC is a generalization and an appropriate benchmark in order to include non-local interactions that preserve the short-wavelength phase-instability. Antiphase coupling in an experimental system was observed in studies of cultured human epileptic astrocytes and supported by simulating the intracellular oscillation via FHN oscillators [15]. For modified Hodgkin–Huxley-type model, different locking patterns in 2D where characterized in Ref. [37] by considering the effect induced by diagonal and non-diagonal neighbors, while antiphase clustered solutions were reported for (antiphase) globally coupled networks of FHN neurons [38].

4.1. Spatiotemporal self-organization

As it is expected, numerical simulations of Eq. (1) show that the dynamics depends both, in the strength D and coupling's range. To have a global view of the dynamics, in Fig. 1 we present the $\{u_i(t)\}$ record of a large subset of neurons for some values of D, k and η. The first row corresponds to $D = 5 \times 10^{-3}$ and $k = 2$ (case A). We can observe in Fig. 1A1 that for vanishingly small noise intensities, there are only small-amplitude homogeneous subthreshold oscillations. These coherent oscillations are induced by the adiabatic signal, and represent the "rest" state (RS), for which $u_i(t) \approx u_j(t)$. Fig. 1A2 shows for $\eta = 9 \times 10^{-9}$ the transition from the rest state to an antiphase state (APS), where an alternated spatial configuration is selected, forming an "…–activated–inhibited–activated–inhibited–…" structure along the network [we call active those cells i for which $u_i(t)$ exceeds some threshold value]. The resulting structure is shown as a stripe pattern. Note that in the APS the activated state is macroscopically occupied and almost half of the neurons remain excited. In particular, this picture shows that the transition to the activated state is not uniform for this level of noise, and a finer-scale analysis of the figure confirms the numerical observation that the jumps take place locally, in groups of few cells which are the "seeds" that force the neighbor to follow the activation process. A similar phenomenon was described for $k = 1$ in Ref. [21]. In Fig. 1A3 we show the same transition to the APS, but now for $\eta = 3 \times 10^{-8}$. In this case the decay to the APS is macroscopic and this kind of pattern (induced in principle by the spatial coupling) has "I-I …-I" defects (I ≡ inhibited) that break the alternance. Structure and defects are both persistent in time. In fact, we observe that the APS persists for some values of noise intensities. Finally, in Fig. 1A4 we show the resulting evolution for a well-developed synchronized regime.

In the second and third rows we consider for $D = 5 \times 10^{-3}$ the couplings with $k = 3$ (case B) and $k = 5$ (case C). In both we see the existence of a static APS, whose alternance is broken by the presence of some defects. For small values of noise intensity the defects remain fixed in the network, while showing a certain degree of mobility for higher noises, as illustrated in Fig. 1B and C.

Finally, the fourth row shows the dynamics observed for $D = 5 \times 10^{-4}$ and $k = 16$ (case D). We can see another path towards noise-sustained synchronization as η increases. Now, the system synchronizes from the RS without an intermediate APS.

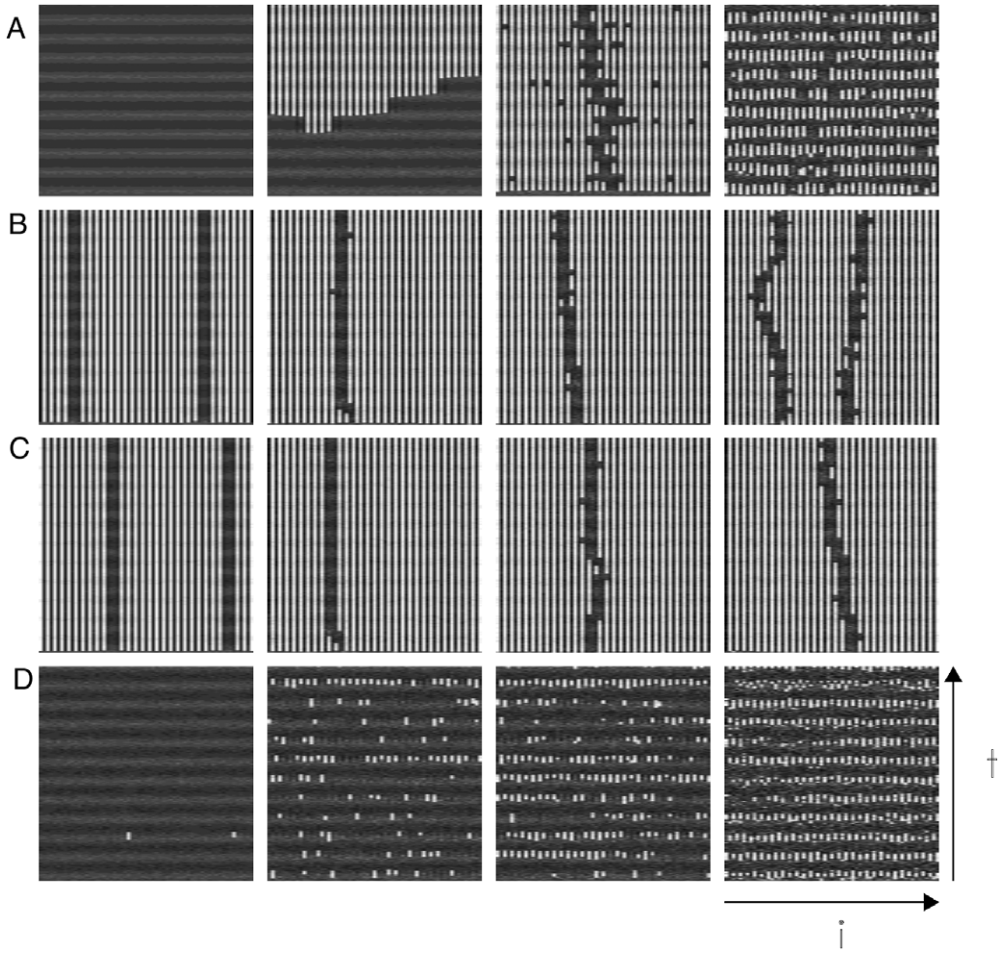

Fig. 1. Time evolution of the u-component for a subset of 60 cells. Time runs on the vertical direction, for $\approx 20\,T$. The u_i values vary approximately between -1.5 and 1.5. Intermediate values are represented in a linear scale of 256 gray levels (maximum in white). The considered cases are: (A) $D = 5 \times 10^{-3}$, $k = 2$ and noises intensities (from left to right): $\eta = 10^{-9}, 9 \times 10^{-9}, 3 \times 10^{-8}, 1.6 \times 10^{-7}$; (B) $D = 5 \times 10^{-3}$, $k = 3$ and $\eta = 7 \times 10^{-9}, 5 \times 10^{-8}, 7 \times 10^{-8}, 1.27 \times 10^{-7}$; (C) $D = 5 \times 10^{-3}$, $k = 5$ and $\eta = 10^{-8}, 5 \times 10^{-8}, 7.5 \times 10^{-8}, 10^{-7}$; (D) $D = 5 \times 10^{-4}$, $k = 16$ and $\eta = 3 \times 10^{-9}, 7 \times 10^{-9}, 10^{-8}, 2.26 \times 10^{-7}$.

4.2. Theoretical description of the dynamics

A characterization of the dynamics can be done by exploiting the properties of the NEP during the time evolution. We consider here, as in Ref. [21], a reduced two-neuron system of variables u_1, u_2, v_1 and v_2, which is a minimal description of an ideal case where all the even nodes on one hand, and all the odd nodes on the other, have the same stochastic phase-space trajectory. For this effective model, the non-local term in Eq. (1) takes the simple form $-kDu_i(t)$ with $i \in \{1, 2\}$. The nullclines of the effective system are useful to clarify different routes to synchronization. In the same sense, the values of their NEP can be used to determine barrier's heights separating attractors. Due to the characteristics of this approximation, the present analysis does not take into account the defects, that will be considered in the next subsection.

Fig. 2 displays for case A the $\mathcal{F}$–level curves in the (u_1, u_2) plane, in the absence of signal. In order to include the fixed points in the two-dimensional representation, the values of the v_i have been adjusted to the slow manifolds $v_i = \beta u_i + C$. Both, the attractors and the saddles, can be obtained either from the intersection of the nullclines or by minimizing $\mathcal{F}(u_1, u_2, v_1, v_2)$. Besides the uniform rest state (which lies along the line $u_1 = u_2$), we can appreciate two excited attractors and two saddle points. Note that the fixed point distribution (in fact the NEP) is symmetric with respect to the $u_1 = u_2$ line, reflecting the u_1–u_2 permutation invariance of the dynamical equations in the two-neuron system. The complete equivalence between symmetric points originates a degeneration in the excited (or antiphase) attractors (u_1 activated, u_2 inhibited or u_2 activated, u_1 inhibited).[2] We remark that the global stability of the attractors is given by the depth of each well respect of the saddle level, and this difference depends on $S(t)$. To illustrate this point, in Fig. 3 we show $\mathcal{F}$ as a function of S for the uniform state – labeled by RS, for the saddles – indicated by SP, and the activated states – indicated by IE. Here $|S| \leq S_0$

[2] Both attractors correspond to two different APSs in the original system, with the "opposite phase" in each node.

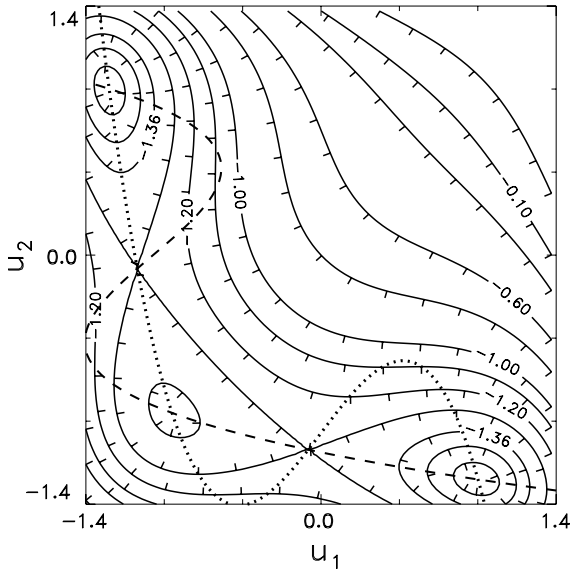

Fig. 2. NEP landscape (in unit of 10^{-5}) in the (u_1, u_2) plane along the $v_i = \beta u_i + C$ lines for the reduced two-neuron system, for $k = 2, D = 5 \times 10^{-3}$ and $S = 0$. The associated nullclines are shown in dotted and dashed lines. The level-line ticks indicate the $\mathcal{F}$-gradient direction. The lines correspond to the levels: -1.43, -1.4, -1.36, -1.2847, -1.2, -1.1, -1, -0.8, -0.6, -0.3, -0.1 and 0.1. Some of them are labeled in the figure.

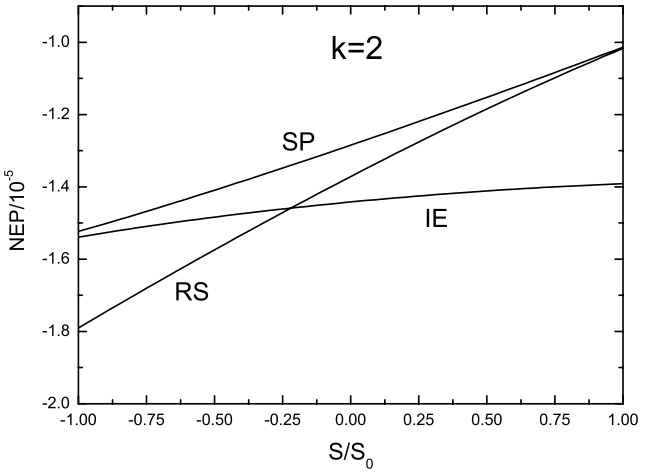

Fig. 3. Value of NEP vs. constant signal for the saddle (SP), excited (IE) and uniform (RS) states for the two-neuron system with $k = 2$ and $D = 5 \times 10^{-3}$. Both saddle points share the same value of $\mathcal{F}$ and the same stands for the excited states.

and there is no intersection between SP and RS lines (the small gap at $S = S_0$ cannot be appreciated in the figure). For each value of S, the global stable state corresponds to the attractor(s) with the lowest values of $\mathcal{F}$, while the other ones are either metastable or unstable states. In particular, for $S(t) = S_0$ the difference in $\mathcal{F}$ between SP and RS is $\Delta\mathcal{F}_a \approx 3 \times 10^{-8}$. For a noise level of this order, the whole system would climb the potential barrier and macroscopically transits to an activated state (IE), that has a lower $\mathcal{F}$ value (see Fig. 1A3). The barrier to scape from the IE states goes from $\Delta\mathcal{F} \approx 37.7 \times 10^{-7}$ at $S = S_0$ to $\Delta\mathcal{F} = \Delta\mathcal{F}_s \approx 1.6 \times 10^{-7}$ at $S = -S_0$. Hence, as $S(t)$ varies the system remains confined in IE, which explains the robustness of the activated state. Thus, $\eta \sim \Delta\mathcal{F}_s$ determines the lowest level of noise necessary to return to the uniform state, so completing the cycle. This noise-induced decay is also associated with a decrease in $\mathcal{F}$. Note that for $\eta \sim \Delta\mathcal{F}_s$, the barrier $\Delta\mathcal{F}_a$ is not significant and the system reaches an excited state during each oscillation of the external signal, namely, it synchronizes (see Fig. 1A4).

For case B we can see an static APS, with some defects that break the alternance, which is macroscopically selected (see Fig. 1B). The nullclines and the NEP levels of the effective system are showed in Figs. 4 and 5, respectively. It can be appreciated that the IE states are present during the complete course of the signal as stable attractors while the SP and the RS collapse at $S \approx 0.28\, S_0$ and change the form of the nullcline. In particular, it is clear that the IE states have the lower potential value, which explains its selection and robustness. A similar analysis can be done in case C, but now the nullclines (not showed) are similar to that of solid line in Fig. 4 for any signal value, i.e., there is not a stable uniform attractor.

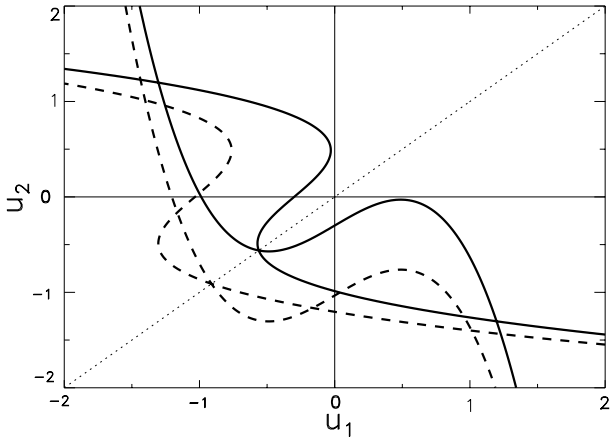

Fig. 4. Nullclines in the (u_1, u_2) plane for the reduced two-neuron system along the $v_i = \beta u_i + C$ lines for $k = 3$ and $D = 5 \times 10^{-3}$. The nullclines for $S = S_0$ and $S = -S_0$ are shown in solid and dashed lines, respectively.

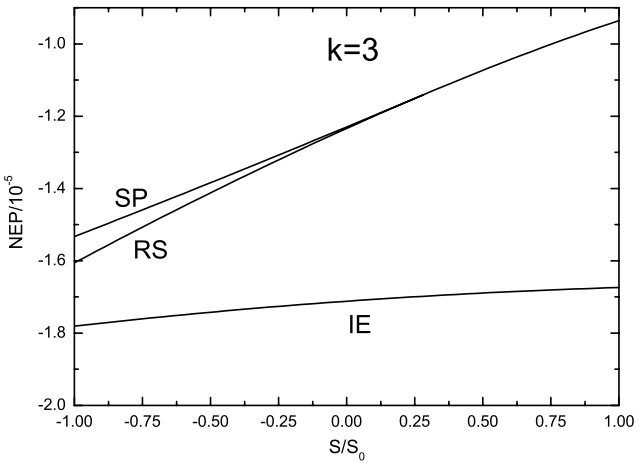

Fig. 5. Value of NEP vs. (constant) signal in the saddle (SP), excited (IE) and uniform (RS) states for the two-neuron system, corresponding to $k = 3$ and $D = 5 \times 10^{-3}$.

The case D shows a different route to synchronization. From the nullclines (see Fig. 6) we can see that only the RS is present – as an attractor – for the full course of the signal. This fact explains the selection of the RS for small noises. The IE states appear only during a fraction of the signal period, and its occupation takes place at $S(t) \sim S_0$, where the barrier $\Delta\mathcal{F}$ between the saddle and the RS is the smallest (see Fig. 7). As the noise increases, this transition becomes more effective, and for $\eta \approx \Delta\mathcal{F} = 2.26 \times 10^{-7}$ the synchronization is complete (see Fig. 1D4). Note that as the signal decreases, the IE states disappear, so the decay from the IE to the RS results deterministic.

As a consequence of the former analysis, the noise-sustained synchronization of systems for which the product of kD is constant, it is expected to be qualitatively and quantitatively similar, at least in the regimes were there are well-developed oscillating APSs. Numerical simulations of Eq. (1) confirm this prediction. We illustrate this point in Fig. 8, where we show the Q-factor vs. η for three different networks that share the same effective system of that considered in Ref. [21] ($k = 1, D = 10^{-2}$). Note that the synchronization is basically the same and in good agreement with the noise intensity predicted by the NEP analysis.[3]

4.3. Stability of defects

As follows from Fig. 1, in cases B and C exist defects that remain static in time for some values of noise, but they get some "mobility" for larger values of η. We also note in simulations that the length L of defects grows as k increases. As in Section 4.2, an exact analysis of the whole system involves a large number of cells. Analytical calculations are hard to do in this context and some approximations are then necessary to extract useful information. In consequence, to model the

[3] See Ref. [21] for definition of Q-factor.

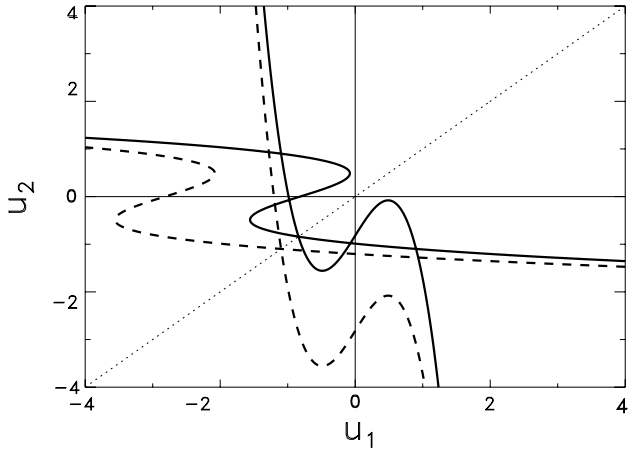

Fig. 6. Nullclines in the (u_1, u_2) plane for the reduced two-neuron system along the $v_i = \beta u_i + C$ lines for $k = 16$ and $D = 5 \times 10^{-4}$. The nullclines for $S = S_0$ and $S = -S_0$ are shown in solid and dashed lines, respectively.

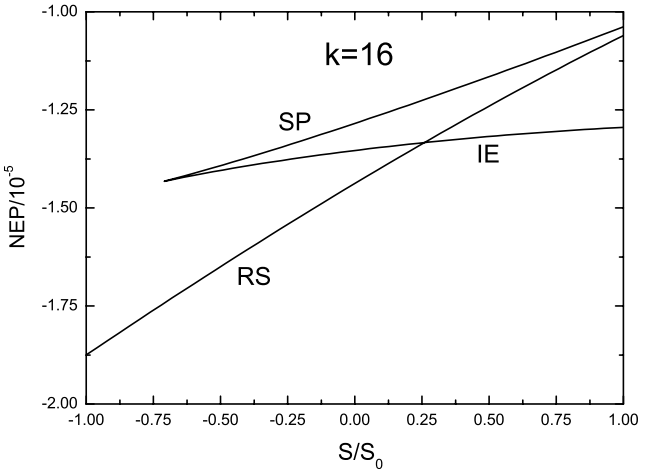

Fig. 7. Value of NEP vs. (constant) signal in the saddle (SP), excited (IE) and uniform (RS) states, for the two-neuron system corresponding to $k = 16$ and $D = 5 \times 10^{-4}$.

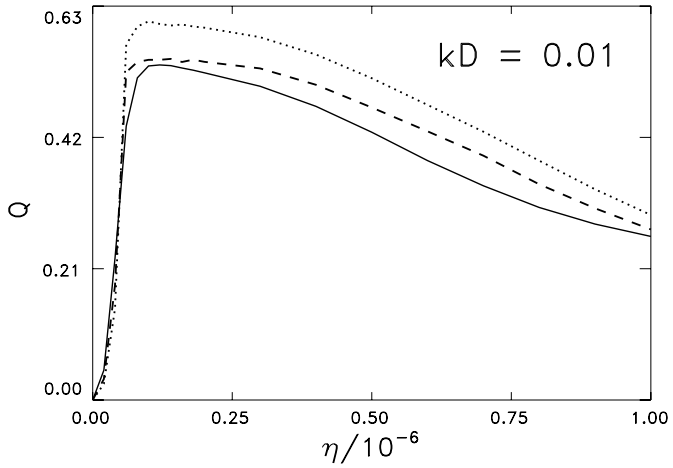

Fig. 8. Q–factor (averaged over 10 realizations) for $k = 1$ (solid line); $k = 10$ (dashed line) and $k = 50$ (dotted line).

defects we consider an idealized configuration with some consecutive inhibited cells, while the rest of the nearby nodes remain in the APS (see scheme in Fig. 10). We approximate all the fixed cell's states in terms of the IE coordinates in the

two-neuron system, that depend on S. Besides, we only consider defects with even length L. In fact, ternary defects are not observed in the simulations, as it is expected if we note that a ternary defect disappears if its central cell changes from inhibited to excited (by minimizing the NEP value). Similar arguments hold for larger odd Ls.

In order to study first the L-dependence with parameters, we calculate the NEP for an L-ary defect in an APS background. After some algebra we obtain

$$\begin{aligned}\mathcal{F}_D = & -(L/2)\Delta\mathcal{F}_s - \frac{2u_E}{\lambda_1}\{\theta^*(L/2-k)(L/2)ku_I + \theta(k-L/2)[k(k+1)u_I - k(k+1-L/2)u_E \\ & + (k^2 - L^2/4 + k + L/2)u_0]\} + \frac{2u_I}{\lambda_1}\{\theta(k-L/2+1)[ku_E(L/2-1) - (L/2)(L/2-1)u_0] \\ & + \theta^*(L/2-k-1)[k(L/2-k-1)u_I + k^2u_E - k(k+1)u_0]\},\end{aligned} \tag{16}$$

where we have excluded some terms which do not depend on L, because we are interested in NEP differences. Here

$$\Delta\mathcal{F}_s = \mathcal{F}_s(u_E, \beta u_E + C) - \mathcal{F}_s(u_I, \beta u_I + C), \tag{17}$$

$$u_0 = \frac{u_E - u_I}{2} \tag{18}$$

and $\theta(x) = 0$ for $x < 0$ and 1 for $x \geq 0$, while $\theta^*(-x) = 1 - \theta(x)$. In Fig. 11 we plot $\mathcal{F}_D(L) - \mathcal{F}_D(L_m)$ at $S = 0$, for different values of k and D. Here L_m is the defect's length where each curve reaches its minimum – i.e. the most probable length L_m. It can be obtained by minimizing the NEP in Eq. (16) resulting[4]

$$L_m = 2k\frac{u_E}{u_E - u_I} + \lambda_1\frac{\Delta\mathcal{F}_s}{(u_E - u_I)^2} + 1. \tag{19}$$

For the considered parameters the second term result negligible and $u_E/(u_E - u_I) \approx 1/2$ for any signal value, therefore

$$L_m \approx k + 1. \tag{20}$$

For example, for $D = 10^{-2}$ and $k = 1$, it results $L_m = 2$ in agreement with the numerical observations in Ref. [21], the same stands for $D = 5 \times 10^{-3}$ and $k = 3$, where we get $L_m = 4$, as seen in Fig. 1B. In general, L_m depend on S, and a small interval of allowed values of L_m are obtained. In this sense, note that basins of attraction of defects are determined by NEP landscape, that also depend on S and a detailed NEP's analysis must be done en each case.

For example, in case B quaternary defects are often observed breaking the alternance of the APS (see Fig. 1B), and from the former analysis they appear as a metastable configuration for $k = 3$. We will estimate here the value of noise intensity for which the defects become mobile. In Fig. 10 we show an APS configuration with a quaternary defect (Fig. 10a) and the same defect displaced two nodes towards the right (Fig. 10b). Note that the minimal displacement of a defect implies that it must move two nodes (right or left) in the APS background, since one-node displacements would imply an exchange of a large number of cells between the excited and the inhibited states (see Fig. 10). In particular, to have a two-node displacement, it is enough that two cells (labeled by C_1 and C_4 in Fig. 10) change their state, while the rest of the nodes remain unaltered. Under these approximations, we have calculated the NEP for a configuration with arbitrary value of cells C_1 and C_4, but for fixed values (inhibited or excited, in agreement with Fig. 10) for the others nodes. Supposing that there is not another defect at a distance minor than $2k$, the NEP is

$$\mathcal{F}_4 = \mathcal{F}_s(u_1, v_1) + \mathcal{F}_s(u_4, v_4) + \frac{2D}{\lambda_1}\{u_1u_4 + (u_1 + u_4)[(k+1)u_I + (k-2)u_E]\}, \tag{21}$$

where the terms that are independent of u_1, v_1, u_4, and v_4 are not included. The first two terms in $\mathcal{F}_4$ correspond to the potentials of isolated nodes C_1 and C_4, while the last term corresponds to the connections of these cells among them and with the rest of the network.

The analysis of the level curves of $\mathcal{F}_4$ allows us to identify maxima, minimums and saddles, which determine the structures of the defects on the APS background. Note that this potential depends on the instantaneous value of the signal $S(t)$. For $S = -S_0$ there are three minima, one symmetrical II and two IE, each one separated by a saddle from the II state (see Fig. 12a). For $S = 0$ a new EE state appears as a metastable minimum and the number of saddles duplicates from 2 to 4 by separating the attractor basins. Simultaneously, a symmetric maximum appears between the saddles by attenuating the transitions between II and EE, and among the IEs. Finally, for $S = S_0$ the II state and the maximum disappear (see Fig. 12c). Note that II states correspond to 6-defects, IE states to quaternary defects, while EE states correspond to binary defects (see Fig. 10).

To quantify the relative stability, in Fig. 13 we show the values of NEP for each fixed point as a function of the signal amplitude. Depending on the instantaneous values of $S(t)$, the minimum of $\mathcal{F}_4$ can be states IE, II or EE, but the last two states do not persist for any value of signal and finally the system evolves to one of the IE states (i.e., to a quaternary defect). Without noise or for small η, the defect remains in this configuration (see Fig. 1B). However, for $\eta \sim \Delta\mathcal{F}_D = 1.27 \times 10^{-7}$ –

[4] The true length is the even number that, being one of the two nearest to L_m given by (19), it has the smallest $\mathcal{F}_D$ value.

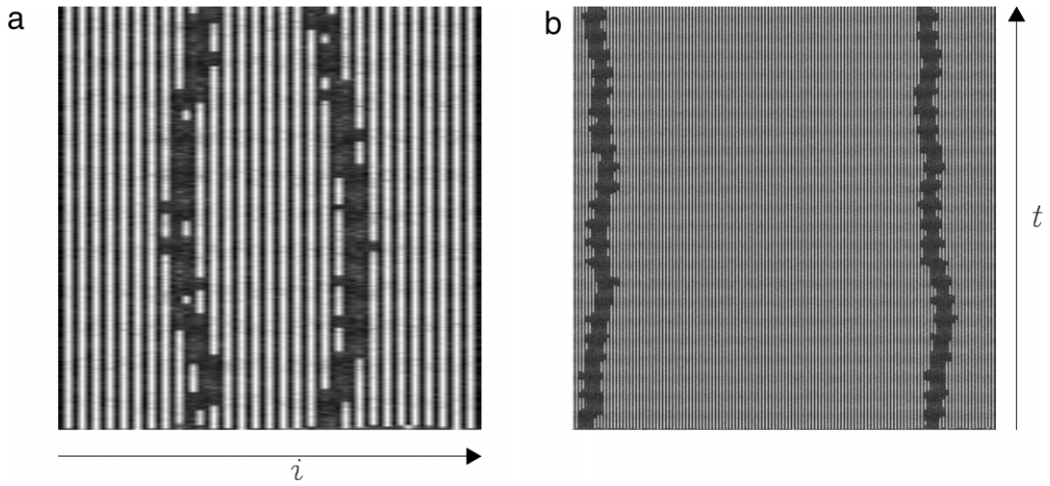

Fig. 9. Time evolution of two defects. (a) $k = 3, D = 5 \times 10^{-3}$ and $\eta = 1.27 \times 10^{-7}$ in a fine scale. Binary, quaternary and 6-ary defects can be observed. Note that quaternary defects are the more frequent, in agreement with theoretical prediction (see also Fig. 1B). (b) Time evolution of the whole system for $k = 10, D = 5 \times 10^{-4}$ and $\eta = 7 \times 10^{-8}$.

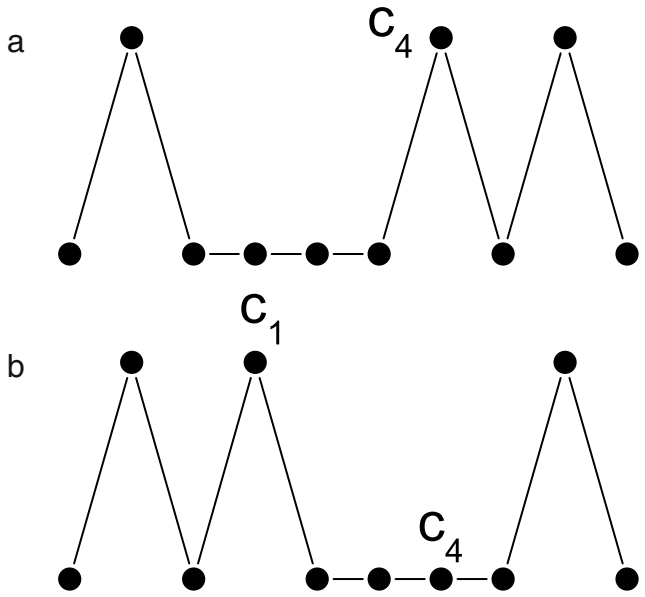

Fig. 10. Scheme of a quaternary defect in an antiphase background. Only nodes C_1 and C_4 change their states when the defect (a) move two cell towards right (b).

NEP difference between SP and IE states at $S = S(0)$ – the system can jump the barrier towards the EE state. As we can see in Fig. 13, this state eventually disappears at $S \approx -0.8\, S_0$ and the system can then decay to the same IE state (i.e., it returns to the departure state), or can decay to the other IE state (i.e., it moves two nodes) or can decay to the II state (by forming a 6-defect).[5] In the same way, the II state disappears at $S \approx 0.44\, S_0$, by allowing new transitions towards states IE or EE. This scenario corresponds to a defect that expands and narrows, following a winding trajectory (see Fig. 9a). This behavior is observed in simulations, even for larger values of k, as we illustrated in Fig. 9b for a case with $k = 10$. We remark that the numerical simulations confirm this scenario in general, and the noise levels predicted by the NEP analysis, in particular.

5. Conclusions

In this work we have analytically calculated the nonequilibrium potential for linearly coupled networks of FitzHugh–Nagumo cells, externally forced by an adiabatic subthreshold harmonic signal and submitted to additive and independent

[5] In fact, the transitions can be also observed before the collapse of attractor EE, for the paths over the maximum which are allowed – for appropriated values of the signal – for $\eta \approx \Delta\mathcal{F}_D$.

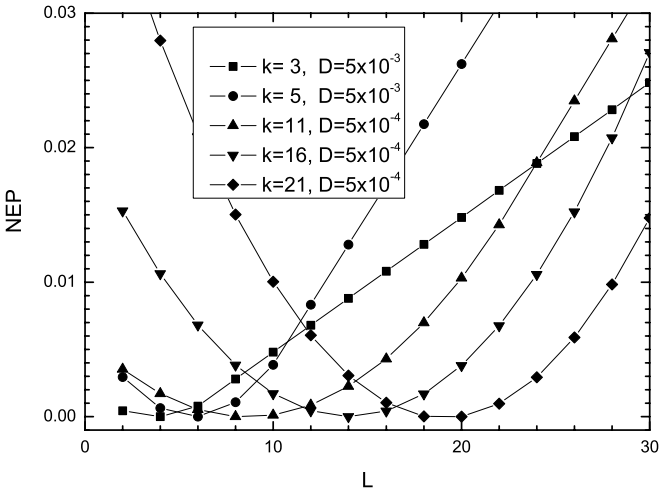

Fig. 11. $\mathcal{F}_D(L) - \mathcal{F}_D(L_m)$ for $S = 0$. The values of k and D are indicated in the figure. Note that $L = 0$ corresponds to a defect with two consecutive excited cells.

Gaussian white noises of the same intensity η. For arbitrary symmetric linear coupling in the activator's variables, we have showed that the nonequilibrium potential is the sum of two terms, the first one is determined by the potential of the isolated nodes – a local component that includes the driving – while the second one (non-local) is determined by the topology of the network and results to be a quadratic form in the activator network's variables, with the coupling matrix elements as coefficients. As a consequence of this structure, conservative and non-conservative components of the flux in the phase-space acquire a non-local character, also determined by the coupling matrix. Integrability conditions – arising from the NEP's derivation – restricts the range of validity of the NEP's expression. Particularly, the linear coupling – arbitrary in principle – is restricted to be symmetric. Nevertheless, we remark that bistable and excitable dynamics can be reached within the aforementioned restriction for arbitrary bidirectional coupling.

The analytical expression for the NEP provide us a way to distinguish the effects produced by the network's topology from the effect induced by the noise. With this theoretical tool at hand, we have investigated the noise-induced dynamics in a regular network with an extended antiphase coupling, where each neuron is symmetrically coupled with its first $2k$ odd-neighbor nodes by means of a negative (antiphase) linear coupling D in the activator's variables.

Two main scenarios were numerically observed. In the first one, the macroscopic activity synchronizes with the external signal for appropriates values of the noise intensity, while in the second one a macroscopic stationary antiphase state is selected. A theoretical characterization of both regimes was done in terms of an effective model with two-coupled cells. In particular, we have showed that the effective NEP determines the levels of noise for global activation and synchronization.

On the one hand, in the first scenario two routes to noise-sustained synchronization were characterized, depending on the state which is stable for null or small noise intensities. In the first route, the synchronization takes place from the antiphase state and all the transitions result noise-sustained, while in the second one the synchronization emerges from the rest state, being the activation noise-sustained, but the decay to the rest state, deterministic. For both routes the dynamics was interpreted in terms of transitions among attractors that change their relative stability (determined by the NEP) due to the driving. As a consequence of the NEP's analysis, the synchronization of regular networks with the same value of the product kD it is expected to be similar, at least for regimes where there are well-developed oscillating states. This fact was numerically confirmed for several networks, in terms of the Q-factors, for both routes of synchronization.

On the other hand, in the second scenario a macroscopic stationary antiphase state is selected. The robustness and stability of the observed structure were explained in terms of the corresponding NEP of the reduced two-neuron system, that identify the selected configuration as the stable attractor. Numerical simulations have showed that the antiphase states present groups of inhibited neurons – defects – that break the alternance. They remain static for small noise intensity but they become mobiles for larger values of noise. By means of the NEP's analysis, we have first determined its most probable length L_m, and then the levels of noise that break the defect's pinning. L_m was estimated by calculating the NEP of an idealized isolated defect. Despite the simplification used, the resulting behavior $L \approx k + 1$ fit accurately the observed values in the numerical simulations. The NEP's analysis has also showed that odd-L defects are unstable while some even-L defect can be expected for small noises. In particular, we have showed that the adiabatic signal changes the landscape of the nonequilibrium potential that confine the defects. For small noise, L_m-defects are expected to be the more frequent, while a number of transitions to another metastable defect's configuration are allowed and can be obtained for appropriate levels of noise.

As we have seen, the NEP provides a powerful framework to study the relation between the network architecture and the effects induced by noise. In particular, it quantifies the levels of noise and determines in each case which transitions are allowed or not, depending on the NEP topology. However, in most realistic systems the analysis is mainly limited by

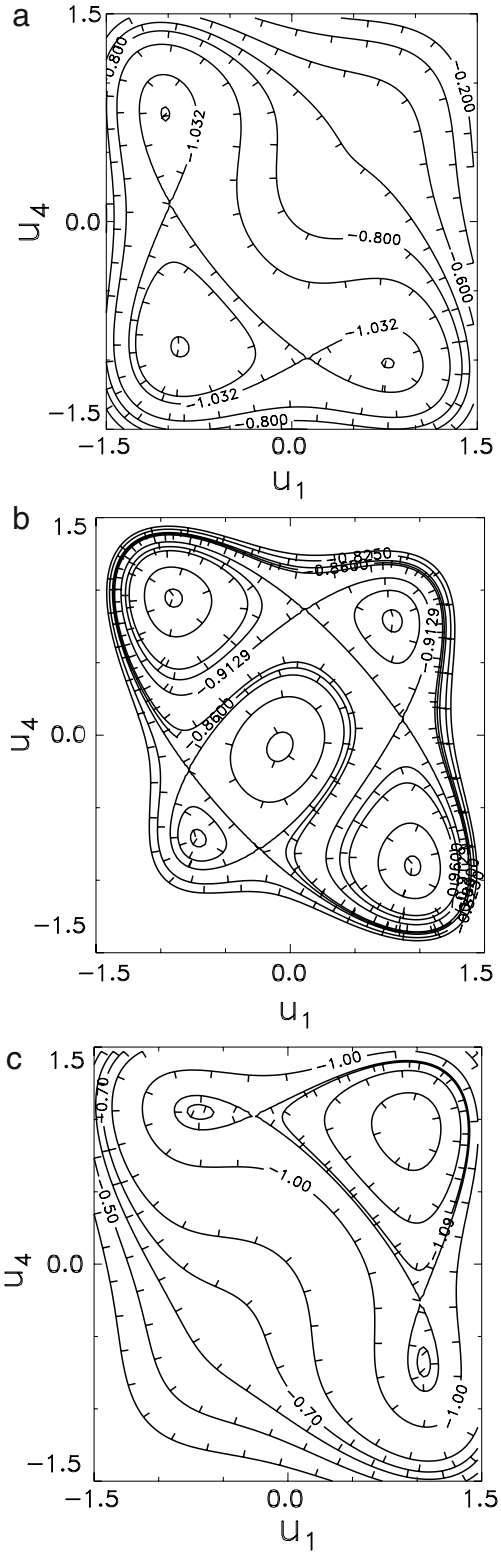

Fig. 12. $\mathcal{F}_4$ landscape in the (u_1, u_4) plane along the $v_i = \beta u_i + C$ lines. Here (a) $S = -S_0$, (b) $S = 0$ and (c) $S = S_0$. The level-line ticks indicate the $\mathcal{F}_4$–gradient direction. Some levels of $\mathcal{F}_4/10^{-5}$ are labeled in the figure.

the intrinsic difficulty to obtain the corresponding NEP. In this sense, the characterization of nonequilibrium potentials in complex networks is an open question, and we hope that our results can be extended to more general (i.e., non-symmetric)

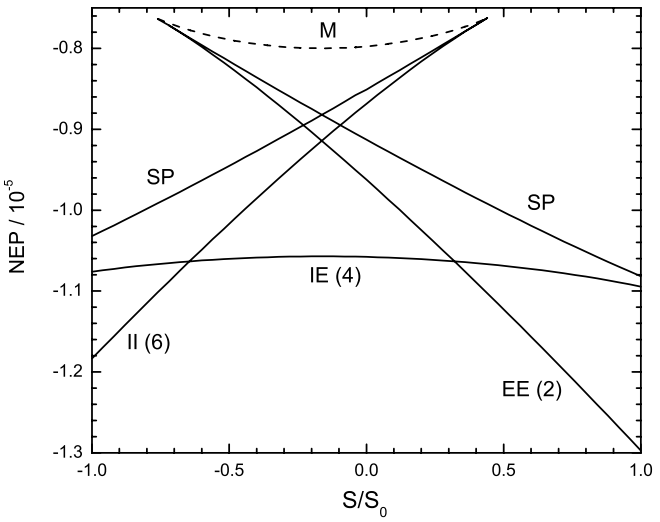

Fig. 13. $\mathcal{F}_4$ from Eq. (21) for the minima (II, IE, EE), saddles (SP) and maximum (M). Neither II nor EE states are present in whole range of signal values. The length of defect in each attractor is indicated between parenthesis.

couplings and systems. Finally, note that the NEP's expression is valid for bidirectional complex networks, for positive as well as for negative spatial coupling and the same approach would be useful for analyzing other kinds of synchronization in networks and continuous systems.

Acknowledgements

We acknowledge financial support from CONICET (Argentina), through Project PIP 5072.

References

[1] A.S. Pikovsky, J. Kurths, Phys. Rev. Lett. 78 (1997) 775.
[2] L. Gammaitoni, P. Hänggi, P. Jung, F. Marchesoni, Rev. Modern Phys. 70 (1998) 223;
K. Weisenfeld, F.J. Jaramillo, Chaos 8 (1998) 539;
T. Wellens, V. Shatokhin, A. Buchleitner, Rep. Progr. Phys. 67 (2004) 45.
[3] C. Zhou, J. Kurths, Phys. Rev. Lett. 78 (1997) 775.
[4] J. Kurths, A. Pikovsky, M. Rosemblum, Synchronization, a Universal Concept in Nonlinear Science, Cambridge Univ. Press, Cambridge, 2001;
C.M. Gray, P. König, A.K. Engel, W. Singer, Nature 338 (1989) 334.
[5] B. Lindner, J. García-Ojalvo, A. Neiman, L. Schimansky-Geier, Phys. Rep. 392 (2004) 321.
[6] A. Arenas, A. Díaz-Guilera, J. Krths, Y. Moreno, C. Zhou, Phys. Rep. 469 (2008) 93.
[7] T. Yanagita, T. Ichinomiya, Y. Oyama, Phys. Rev. E 72 (2005) 056218.
[8] L. Glass, P. Hunter, A. McCulloch (Eds.), Theory of Heart, Springer Verlag, Berlin, 1991.
[9] D.T. Kaplan, et al., Phys. Rev. Lett 76 (1996) 4074.
[10] J.R. Clay, J. Comput. Neurosci. 15 (2003) 43.
[11] R. Toral, C.R. Mirasso, J.D. Gunton, Erophys. Lett. 61 (2003) 162.
[12] U. Ernst, K. Pawelzik, T. Heisel, Phys. Rev. E 57 (1998) 2150.
[13] C. Sagui, R.C. Desai, Phys. Rev. Lett. 74 (1995) 1119.
[14] Y. Nakamura, F. Tominaga, T. Munakata, Phys. Rev. E 49 (1994) 4849.
[15] G. Balázsy, A. Cornell-Bell, A.B. Neimal, F. Moss, Phys. Rev. E 64 (2001) 041912.
[16] E.V. Pankratovas, et al., Phys. Lett. A 344 (2006) 43.
[17] H. Kitajima, J. Kurths, Chaos 15 (2005) 023704.
[18] E.I. Volkov, et al., Phys. Rev. E 68 (2003) 061112.
[19] A. Neiman, et al., Phys. Rev. Lett. 83 (1999) 4896.
[20] G. Izús, R.R. Deza, H.S. Wio, Phys. Rev. E 58 (1998) 93.
[21] G. G Izús, A.D. Sánchez, R.R Deza, Physica A 388 (2009) 967.
[22] R Graham, in: E. Tirapegui, D. Villarroel (Eds.), Instabilities and Nonequilibrium Structures, in: Mathematics and its applications, D. Reidel, Dordrecht, 1987, pp. 271–290.
[23] H.S. Wio, R.R. Deza, Eur. Phys. J. Special Topics 146 (2007) 111.
[24] B. von Haeften, G. Izús, H.S. Wio, Phys. Rev. E 72 (2005) 021101.
[25] B. von Haeften, R.R. Deza, H.S. Wio, Phys. Rev. Lett. 84 (2000) 404.
[26] B. von Haeften, G. Izús, S. Mangioni, A.D. Sánchez, H.S. Wio, Phys. Rev. E 69 (2004) 21107.
[27] B. Lindner, L. Schimansky-Geier, Phys. Rev. E 60 (1999) 7270.
[28] V.A. Makarov, V.I. Nekorkin, M.G. Velarde, Phys. Rev. Lett. 86 (2001) 3431;
R. Toral, C.R. Mirasso, J.D. Gunton, Europhys. Lett. 61 (2003) 162.
[29] R. Fitzhugh, Biophys. J. 1 (1961) 445;
J.S. Nagumo, S. Arimoto, S. Yoshizawa, PROC. IRE 50 (1962) 2061.
[30] C. Koch, Biophysics of Computation: Information Processing in Single Neurons, Oxford, New York, 1999.

[31] N.B. Janson, A.G. Galanov, E. Schöll, Phys. Rev. Lett. 93 (2004) 010601.
[32] H. Risken, The Fokker–Planck Equation, Springer-Verlag, Berlin, 1989 (Chapter 3).
[33] A. Sherman, J. Rinzel, Proc. Natl. Acad. Sci. USA 89 (1992) 2471.
[34] G. Izús, R.R. Deza, H.S. Wio, Comput. Phys. Comm. 121–122 (1999) 406.
[35] S. Bouzat, H.S. Wio, Phys. Lett. A 247 (1998) 297.
[36] G. Izús, R. Deza, A.D. Sánchez, AIP Conf. Proc. 887 (2007) 89.
[37] O. Weihberger, S. Bahar, Phys. Rev. E 76 (2007) 011910.
[38] C.G. Assisi, V.K. Jirsa, J.A. Scott-Kelso, Phys. Rev. Lett. 94 (2005) 018106.